Different contributions of nonmuscle myosin IIA and IIB to the organization of stress fiber subtypes in fibroblasts

Masahiro Kuragano[a], Taro Q. P. Uyeda[b], Keiju Kamijo[c], Yota Murakami[a,d], and Masayuki Takahashi[a,d,*]
[a]Graduate School of Chemical Science and Engineering, Hokkaido University, Sapporo, Hokkaido 060-8628, Japan; [b]Department of Physics, Faculty of Science and Engineering, Waseda University, Tokyo 169-8555, Japan; [c]Department of Anatomy, Faculty of Medicine, Tohoku Medical and Pharmaceutical University, Sendai, Miyagi 981-8558, Japan; [d]Department of Chemistry, Faculty of Science, Hokkaido University, Sapporo, Hokkaido 060-0810, Japan

ABSTRACT **Stress fibers (SFs) are contractile, force-generating bundled structures that can be classified into three subtypes, namely ventral SFs (vSFs), transverse arcs (TAs), and dorsal SFs. Nonmuscle myosin II (NMII) is the main component of SFs. This study examined the roles of the NMII isoforms NMIIA and NMIIB in the organization of each SF subtype in immortalized fibroblasts. Knockdown (KD) of NMIIA (a major isoform) resulted in loss of TAs from the lamella and caused the lamella to lose its flattened shape. Exogenous expression of NMIIB rescued this defect in TA formation. However, the TAs that formed on exogenous NMIIB expression in NMIIA-KD cells and the remaining TAs in NMIIB-KD cells, which mainly consisted of NMIIB and NMIIA, respectively, failed to rescue the defect in lamellar flattening. These results indicate that both isoforms are required for the proper function of TAs in lamellar flattening. KD of NMIIB resulted in loss of vSFs from the central region of the cell body, and this defect was not rescued by exogenous expression of NMIIA, indicating that NMIIA cannot replace the function of NMIIB in vSF formation. Moreover, we raised the possibility that actin filaments in vSFs are in a stretched conformation.**

Monitoring Editor
Yu-Li Wang
Carnegie Mellon University

Received: Apr 5, 2017
Revised: Feb 14, 2018
Accepted: Feb 16, 2018

INTRODUCTION

Stress fibers (SFs) are contractile, force-generating bundled structures consisting mainly of actin filaments, nonmuscle myosin II (NMII) filaments, and α-actinin. These fibers are prominent in cultured mesenchymal cells, such as fibroblasts and osteoblasts, as well as in cultured smooth muscle cells. There are three subtypes of SFs, namely, ventral SFs (vSFs), transverse arcs (TAs), and dorsal SFs (dSFs), which are categorized based on their distinct subcellular localizations and termination sites (Figure 1A) (Small *et al.*, 1998; Tojkander *et al.*, 2012; Burridge and Wittchen, 2013; Vallenius, 2013; Skau and Waterman, 2015; Kassianidou and Kumar, 2015). vSFs are tightly packed actomyosin bundles located along the basal surface of cells. Both ends of vSFs link to focal adhesions (FAs). vSFs mediate stable adhesion with the underlying substrate and also facilitate contraction of the rear of migrating cells. Both TAs and dSFs are present in highly protrusive cells that possess flat lamellae. TAs are curved actomyosin bundles that form beneath the dorsal surface of lamellae. They undergo centripetal flow toward the cell body and eventually disappear near the end of the lamella (Heath, 1983; Burnette *et al.*, 2011; Hu *et al.*, 2017). TAs, which do not directly link to FAs at both ends, mediate the periodic protrusion and retraction of the leading edge of cells during migration (Burnette *et al.*, 2011). dSFs are relatively short actin filament bundles that are prominent in lamellae. They link to FAs only at the distal end of the ventral surface and often connect to TAs at right angles at the proximal end of the dorsal surface. Some dSFs connect to regions close to the ends of TAs (Hotulainen and Lappalainen, 2006). dSFs transmit force, which is generated by the contraction of TAs, to substrates (Oakes *et al.*, 2012; Kovac *et al.*, 2013; Burnette *et al.*, 2014).

This article was published online ahead of print in MBoC in Press (http://www.molbiolcell.org/cgi/doi/10.1091/mbc.E17-04-0215) on February 19, 2018.

*Address correspondence to: Masayuki Takahashi (takahash@sci.hokudai.ac.jp).

Abbreviations used: 1P-RLC, monophosphorylated regulatory light chain at Ser-19; 2P-RLC, diphosphorylated regulatory light chain at Thr-18 and Ser-19; dSF, dorsal stress fiber; FA, focal adhesion; FBS, fetal bovine serum; KD, knockdown; NMHC, nonmuscle myosin heavy chain; NMII, nonmuscle myosin II; PBS, phosphate-buffered saline; RLC, regulatory light chain; S1, subfragment 1; SF, stress fiber; siRNA, small interfering RNA; TA, transverse arc; vSF, ventral stress fiber.

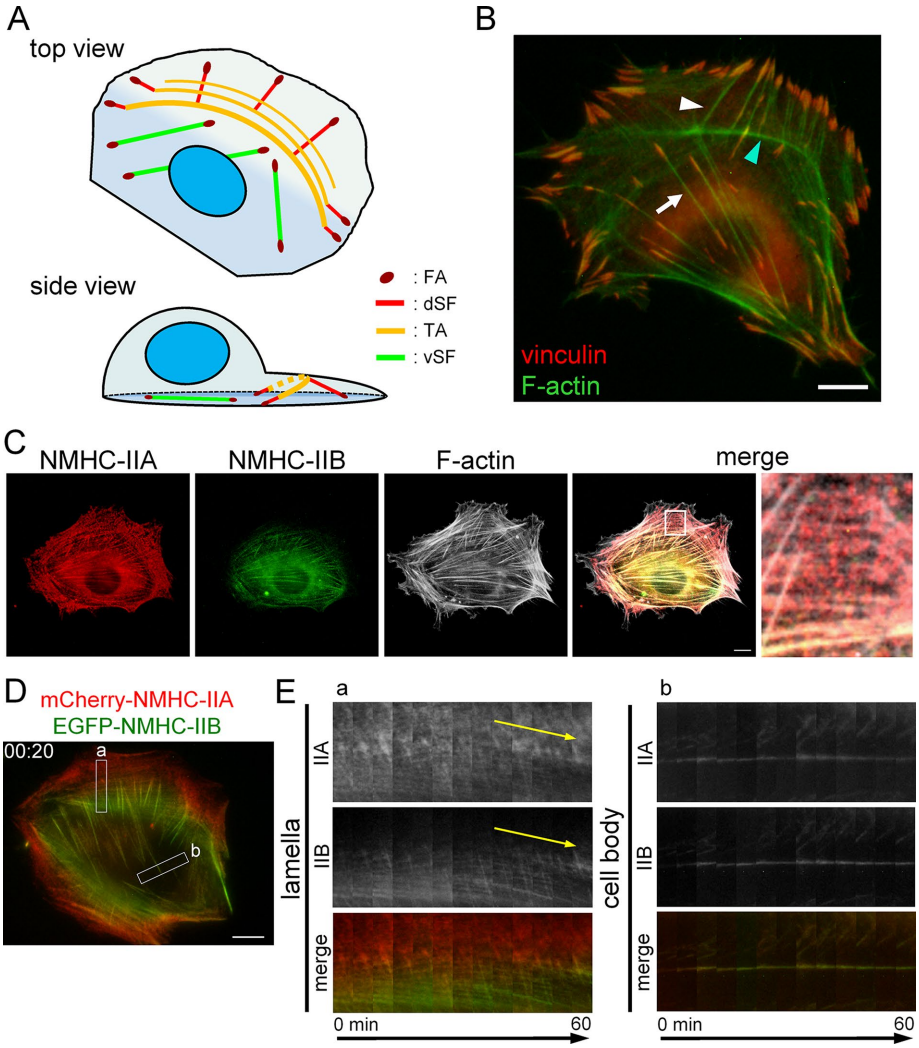

FIGURE 1: Organization and dynamics of NMIIA and NMIIB in SF subtypes. (A) Schematic representation of the SF subtypes in protrusive cells. In the side view, only one of each SF subtype is illustrated for simplification. (B) SV1 cells were fixed and stained with an anti-vinculin monoclonal antibody (red) and FITC-phalloidin (green). The white arrow and white arrowhead point to a representative vSF and dSF, respectively. The cyan arrowhead points to a representative TA. (C) SV1 cells were fixed and stained with an Alexa Fluor 596–conjugated anti–NMHC-IIA polyclonal antibody (red), an Alexa Fluor 488–conjugated anti–NMHC-IIB polyclonal antibody (green), and Alexa Fluor 350-phalloidin (gray). The enlarged image of the boxed region in the merged image shows the lamellar region. Note that red puncta corresponding to NMIIA were distributed in TAs. (D) Still image showing mCherry-NMHC-IIA and EGFP-NMHC-IIB fluorescence from Supplemental Movie S3 (merged image) at 20 min. (E) Kymographs generated from the boxed regions in D. Left (box a) and right (box b) panels exhibit the centripetal flow of TAs in the lamella and less mobile vSFs in the cell body, respectively. Yellow arrows emphasize the slopes indicating the centripetal flow of TAs. All images were captured using a conventional fluorescence microscope. Bar, 10 μm.

The main component of SFs, NMII, plays a key role in diverse types of cellular motility by generating contractile forces together with actin filaments (Conti and Adelstein, 2008; Vicente-Manzanares *et al.*, 2009). NMII is composed of a pair of heavy chains and two pairs of light chains. This motor protein comprises two globular heads, which are involved in motor activity, and a long rodlike tail, which is involved in filament formation. The motor activity and filament formation of NMII are dependent on phosphorylation of its regulatory light chain (RLC) subunit at Thr-18 and Ser-19 by several kinases such as ROCK/Rho-kinase and myosin light chain kinase (Vicente-Manzanares *et al.*, 2009; Heissler and Manstein, 2013). Activation of NMII by this phosphorylation is important for the assembly and maintenance of SFs and for the maturation of FAs, which are mediated by Rho-kinase signaling. There are three isoforms of nonmuscle myosin heavy chain (NMHC) in mammalian cells, namely NMHC-IIA, NMHC-IIB, and NMHC-IIC. NMIIA, NMIIB, and NMIIC are homodimeric with respect to their heavy chain subunits (Vicente-Manzanares *et al.*, 2009; Heissler and Manstein, 2013; Ma and Adelstein, 2014). Moreover, NMIIA localizes throughout cells, whereas NMIIB is generally excluded from the peripheral region of stationary cells and the anterior lamellar region of migrating cells (Maupin *et al.*, 1994; Kolega, 1998; Saitoh *et al.*, 2001; Lo *et al.*, 2004; Rossier *et al.*, 2010). In vitro studies revealed that these isoforms have distinct motor properties (Kovács, Wang, *et al.*, 2003; Kovács *et al.*, 2007; Rosenfeld *et al.*, 2003; Wang, Kovács, *et al.*, 2003). NMIIA exhibits higher motor activity for translocation of actin filaments than NMIIB. On the other hand, NMIIB exhibits slow ADP release and high ADP affinity, resulting in a high duty ratio (the fraction of time that the NMII head spends in the strong actin-binding states during the ATPase cycle). Based on these distinct motor properties, NMIIA and NMIIB have been suggested to mainly function in the translocation (motor property) and cross-linking (structural property) of actin filaments, respectively (Wang, Kovács, *et al.*, 2003; Kovács *et al.*, 2007; Vicente-Manzanares *et al.*, 2009; Rossier *et al.*, 2010; Heissler and Manstein, 2013; Stam *et al.*, 2015).

Although several studies demonstrated that both NMIIA and NMIIB are involved in the formation of SFs and FAs (Wei and Adelstein, 2000; Cai *et al.*, 2006; Sandquist *et al.*, 2006; Betapudi *et al.*, 2006; Even-Ram *et al.* 2007; Vicente-Manzanares *et al.*, 2007, 2011; Betapudi, 2010; Jorrisch *et al.*, 2013; Chang and Kumar, 2015), most of them did not focus on the categorization of SF subtypes. On the other hand, many important findings on the function of NMII in the organization of SF subtypes have been reported (e.g., Hotulainen and Lappalainen, 2006; Oakes *et al.*, 2012; Kovac *et al.*, 2013; Burnette *et al.*, 2014; Schulze *et al.*, 2014). However, most of these studies did not address the different roles of NMIIA and NMIIB in the organization of each SF subtype.

To elucidate whether NMII isoforms have distinct roles in the organization of SF subtypes in fibroblasts, we knocked down each isoform individually. Our results revealed that NMIIA and NMIIB are required for the formation of TAs and vSFs, respectively. Furthermore, we illustrated the roles of NMII isoforms in lamellar flattening and also raised the possibility that actin filaments in vSFs are in a stretched conformation.

RESULTS

NMIIA and NMIIB localize to SF subtypes differently

To investigate the involvement of NMIIA and NMIIB in the organization of SF subtypes, we used MRC-5 SV1 TG1 cells (SV1 cells) because they contain each SF subtype as described below (Figure 1A). The level of NMHC-IIC was below the detection limit of immunoblotting in this cell line (unpublished data). In addition, SV1 cells migrate very slowly, which allows cytoskeletal dynamics to be easily studied via time-lapse observation. Immunofluorescence revealed that vSFs, TAs, and dSFs were present in SV1 cells (Figure 1B). We next analyzed the dynamics of each SF subtype in SV1 cells expressing mCherry-actin and EGFP-vinculin (Supplemental Movies S1 and S2 and Supplemental Figure S1). TAs exhibited dynamic centripetal flow in lamellae, whereas vSFs were less mobile in cell bodies. On the basis of these results, we confirmed the presence of all three SF subtypes and their dynamic properties in SV1 cells.

Next, we visualized endogenous NMIIA and NMIIB in each of the three SF subtypes. NMIIA localized to SFs throughout cells, whereas NMIIB was excluded from the peripheral region (Figure 1C). The localization patterns of NMIIA and NMIIB in SV1 cells were similar to those observed in other cells (Maupin *et al.*, 1994; Saitoh *et al.*, 2001; Lo *et al.*, 2004; Rossier *et al.*, 2010; Beach *et al.*, 2014; Shutova *et al.*, 2014). Focusing on the lamellar region, NMIIA localized in all TAs as puncta, whereas NMIIB predominantly localized to proximal TAs. This difference in the localization patterns of NMIIA and NMIIB in TAs was similar to that observed in U-2 OS cells (Vallenius, 2013; Beach *et al.*, 2014). We next examined the dynamics of NMIIA and NMIIB in cells expressing mCherry-NMHC-IIA and EGFP-NMHC-IIB (Supplemental Movie S3 and Figure 1D). Both isoforms localized in TAs exhibited dynamic centripetal flow in lamellae, whereas those localized in vSFs were less dynamic in cell bodies. Kymographs indicated that NMIIB was gradually incorporated into TAs that already contained NMIIA during centripetal flow (Figure 1E). These results suggest that nascent distal TAs are formed by only NMIIA and that gradual incorporation of NMIIB is associated with the maturation of TAs in fibroblasts.

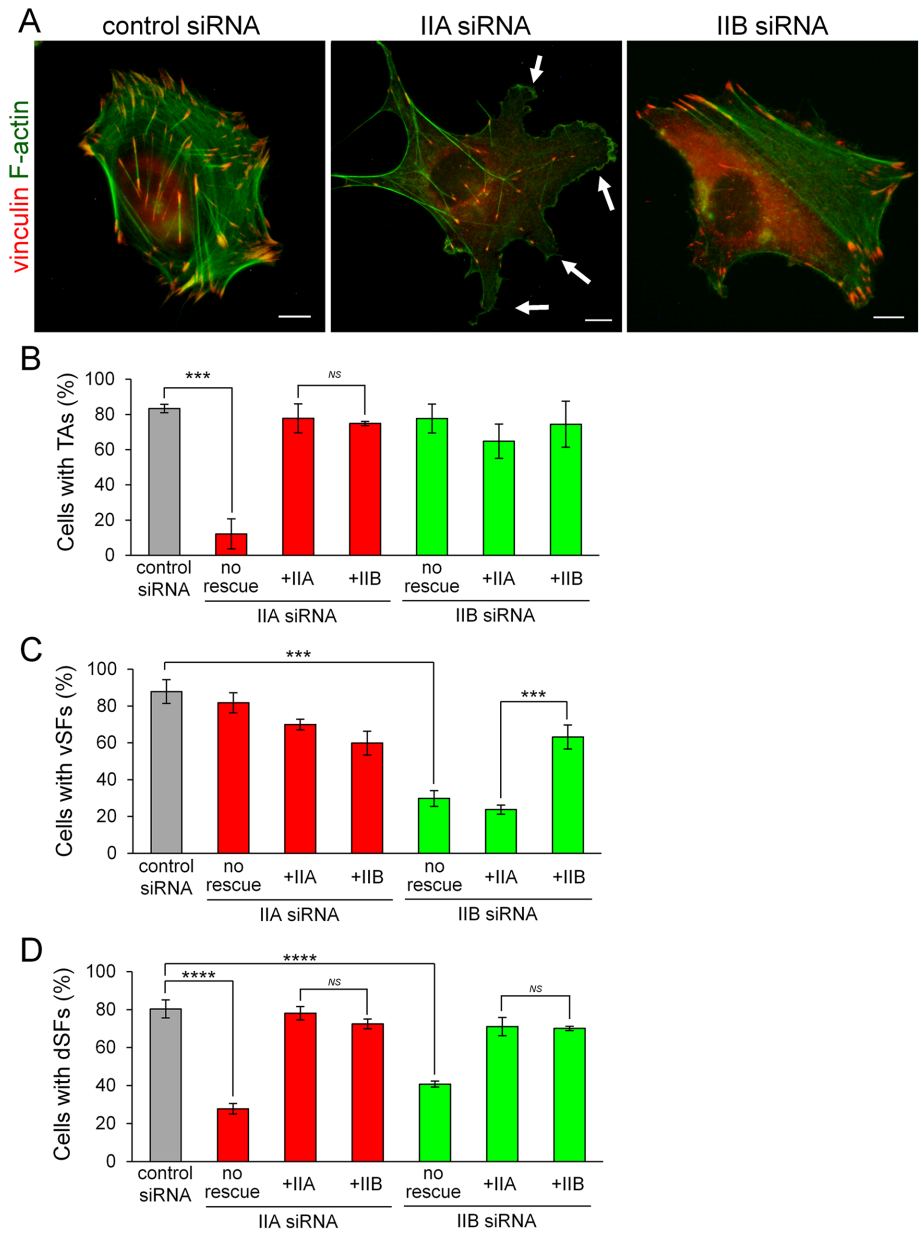

FIGURE 2: NMIIA and NMIIB are required for the formation of TAs and vSFs, respectively. (A) SV1 cells treated with the indicated siRNAs were fixed and stained with an anti-vinculin monoclonal antibody (red) and FITC-phalloidin (green). White arrows point to aberrant protrusions at the leading edge. Bar, 10 μm. (B–D) Rescue experiments of the defects in NMIIA-KD and NMIIB-KD cells on exogenous expression of each NMII isoform. Percentages of cells exhibiting TAs (B), vSFs (C), and dSFs connecting to TAs at right angles (D) on treatment with the indicated siRNAs. Note that NMHC-IIB rescued the defect in TA formation in NMIIA-KD cells, but NMHC-IIA failed to rescue the defect in vSF formation in NMIIB-KD cells. Data represent the mean ± SD from three independent experiments with $n > 30$ cells per experiment. ***$p < 0.0005$, ****$p < 0.00005$.

NMIIA and NMIIB are required for the formation of TAs and vSFs, respectively

To assess the involvement of NMIIA and NMIIB in the formation of SF subtypes, we investigated the effects of knockdown (KD) of each NMHC-II isoform using isoform-specific small interfering RNAs (siRNAs). Immunoblot analysis confirmed that transfection of siRNAs targeting NMHC-IIA and NMHC-IIB reduced endogenous expression of the corresponding isoform (Supplemental Figure S2, A and B). We previously demonstrated that expression of NMIIA is ~15-fold higher than that of NMIIB in SV1 cells (Sato *et al.*, 2007). Therefore, it should be noted that the total amount of NMII in SV1 cells was greatly decreased by KD of NMIIA but was not markedly affected by KD of NMIIB.

Figure 2A shows representative images of siRNA-treated cells stained with an anti-vinculin antibody and fluorescein isothiocyanate (FITC)-phalloidin. The three SF subtypes were observed in control siRNA-treated cells. NMIIA KD resulted in loss of

TAs, as well as dSFs connecting to TAs at right angles, from the lamella and the formation of aberrant protrusions at the extending edge of cells. Although vSFs were observed in the cell body on NMIIA KD, some were abnormally branched. On the other hand, NMIIB KD resulted in loss of vSFs from the cell body and the formation of relatively straight SFs in the lamella. We considered these relatively straight SFs to be TAs connecting to dSFs at both ends because they aligned and oriented toward the extending edge in parallel and exhibited centripetal flow, as mentioned later. In addition, almost all dSFs connecting to TAs at right angles disappeared in NMIIB-KD cells. We confirmed that the phenotypes of siRNA-treated cells were caused by KD of each isoform (Supplemental Figure S2C). vSFs in NMIIA-KD cells were immunoreactive for only NMIIB, whereas TAs in NMIIB-KD cells were immunoreactive for only NMIIA. We quantified the percentages of NMIIA-KD and NMIIB-KD cells exhibiting each SF subtype. Only 12% of NMIIA-KD cells formed TAs (Figure 2B), whereas only 30% of NMIIB-KD cells formed vSFs (Figure 2C). The percentage of cells displaying dSFs connecting to TAs at right angles was decreased on KD of NMIIA or NMIIB (Figure 2D). These results indicate that KD of each NMII isoform has distinct effects on the organization of SF subtypes. Specifically, NMIIA and NMIIB are required for the formation of TAs and vSFs, respectively.

To assess the properties of the remaining SFs in NMIIA-KD and NMIIB-KD cells, we analyzed the dynamics of exogenously expressed mCherry-actin and EGFP-vinculin (Supplemental Movies S4–S9 and Supplemental Figure S3A). The remaining vSFs became mobile in NMIIA-KD cells (Supplemental Figure S3B). In addition, FAs connected to the ends of vSFs were smaller in NMIIA-KD cells than in control cells (Figure 2A and Supplemental Figure S3C). The formation and maturation of SFs and FAs are dependent on the tension applied to them (Chrzanowska-Wodnicka and Burridge, 1996; Gardel *et al*., 2010); therefore, vSFs in NMIIA-KD cells might be unable to generate normal contractile force. The remaining TAs in NMIIB-KD cells exhibited centripetal flow; however, the flow rate was slower than in control cells (Supplemental Figure S3, B and D), suggesting that these relatively straight TAs also have defects.

To test whether the alteration of SF subtypes organization in NMIIA-KD and NMIIB-KD cells is due to the lack of the specific isoform, we performed KD-rescue experiments using siRNA-insensitive EGFP-NMHC isoforms that were expressed under the regulation of a CMV promoter. Immunoblot analysis confirmed the expression of exogenous EGFP-NMHC-IIA and EGFP-NMHC-IIB (Supplemental Figure S4). As expected, expression of exogenous EGFP-NMHC-IIA and EGFP-NMHC-IIB rescued the defects of NMIIA-KD and NMIIB-KD cells, respectively (Figure 2, B–D, and Supplemental Figure S5). Specifically, TAs formed in NMIIA-KD cells expressing EGFP-NMHC-IIA and vSFs formed in NMIIB-KD cells expressing EGFP-NMHC-IIB. EGFP-NMHC-IIB was able to localize in the distal region of the lamella and rescue the TA formation defect in NMIIA-KD cells. This indicates that NMIIB can form TAs when it is present in excess and localizes in the distal region of the lamella. However, exogenous EGFP-NMHC-IIA failed to rescue the defects of NMIIB-KD cells. Specifically, vSFs did not form in NMIIB-KD cells, even in the presence of excess exogenous EGFP-NMHC-IIA. This result indicates that the formation of vSFs is dependent on NMIIB.

Activation of NMII by phosphorylation of its RLC subunit is critical for the formation of SFs (Chrzanowska-Wodnicka and Burridge, 1996; Totsukawa *et al*., 2000). We examined the effects of KD of each NMHC-II isoform on the phosphorylation status of the RLC (Supplemental Figure S6). Levels of both monophosphorylated RLC at Ser-19 (1P-RLC) and diphosphorylated RLC at Thr-18 and Ser-19 (2P-RLC) were decreased in NMIIA-KD cells. This decrease in RLC phosphorylation could be explained by a reduction in the total amount of NMII or by a loss of motor activity specific to NMIIA. Levels of 1P-RLC and 2P-RLC were also decreased in NMIIB-KD cells, despite the fact that most NMII molecules (i.e., NMIIA) remained, indicating that NMIIB is required for proper phosphorylation of the RLC. These results illustrate that proper activation of NMII isoforms is required for the formation of TAs and vSFs.

Both NMIIA and NMIIB are required to maintain lamellar flattening

Burnette *et al*. (2014) recently provided new insights into the function of TAs. They showed that TAs are required to maintain the thin and flattened shape of the lamella by mechanically coupling with dSFs (Burnette *et al*., 2014) and also indicated that NMIIA is important for this lamellar flattening. However, NMIIB also localized to proximal TAs, in addition to NMIIA (Figure 1, C and D), which prompted us to investigate the involvement of NMIIB in lamellar shape. We compared the height of the peripheral region in each siRNA-treated cell using confocal microscopy (Figure 3, A and B, and Supplemental Movie S10). TAs, as well as vSFs, were observed in the ventral plane close to the basal region in control siRNA-treated cells, indicating that these cells had very thin and flattened lamellae. Although superresolution three-dimensional (3D) microscopy can separate the dorsal surface from the ventral surface of the lamella (Burnette *et al*., 2014), the conventional confocal microscope used in this study produced images that showed these surfaces within the same plane of control cells. In NMIIA-KD cells, TAs were not observed, and the peripheral region was thicker. These results demonstrate that TAs are required for lamellar flattening in SV1 cells, consistent with findings in U-2 OS cells (Burnette *et al*., 2014). In NMIIB-KD cells, however, the peripheral region was thicker even in the presence of TAs. Although both ends of TAs were observed in the ventral plane of lamellae, the central region of TAs was observed in the dorsal plane ~2 μm above the ventral plane (see the NMIIB-KD cell in Figure 3A). This result indicates that TAs lacking NMIIB cannot function properly in lamellar flattening.

Next, we performed KD-rescue experiments to determine whether the observed effects are due to the lack of the specific NMII isoform (Figure 3, B and C, and Supplemental Movies S11 and S12). We measured the height of lamellae in cells treated with each siRNA and expressing exogenous EGFP-NMHC-IIA or EGFP-NMHC-IIB. Lamella height in NMIIA-KD and NMIIB-KD cells was decreased to a level comparable to that in control cells on expression of EGFP-NMHC-IIA and EGFP-NMHC-IIB, respectively. On the other hand, lamella height was not decreased in NMIIA-KD and NMIIB-KD cells on exogenous expression of EGFP-NMHC-IIB and EGFP-NMHC-IIA, respectively, even though TAs formed in these cells. In summary, the defects were not rescued by expression of the other isoform, suggesting that TAs lacking NMIIA or NMIIB cannot function in lamellar flattening. Although dSFs formed in NMIIA-KD and NMIIB-KD cells expressing exogenous NMIIB and NMIIA, respectively, a flattened lamella still failed to form. The presence of dSFs itself is probably not enough for lamellar flattening. Therefore, the presence of both NMIIA and NMIIB in TAs is necessary to maintain the thin and flattened shape of lamellae.

To investigate TA defects in NMIIB-KD cells, we examined the arrangement of NMII filaments in TAs during centripetal flow. NMII filaments in TAs align at regular intervals, and the distance between the respective filaments decreases on contraction of TAs during centripetal flow (Burnette *et al*., 2014). Furthermore, NMII filaments form a stack by aligning their long axes parallel to the extending edge in lamellae during centripetal flow (Burnette *et al*., 2014; Fenix

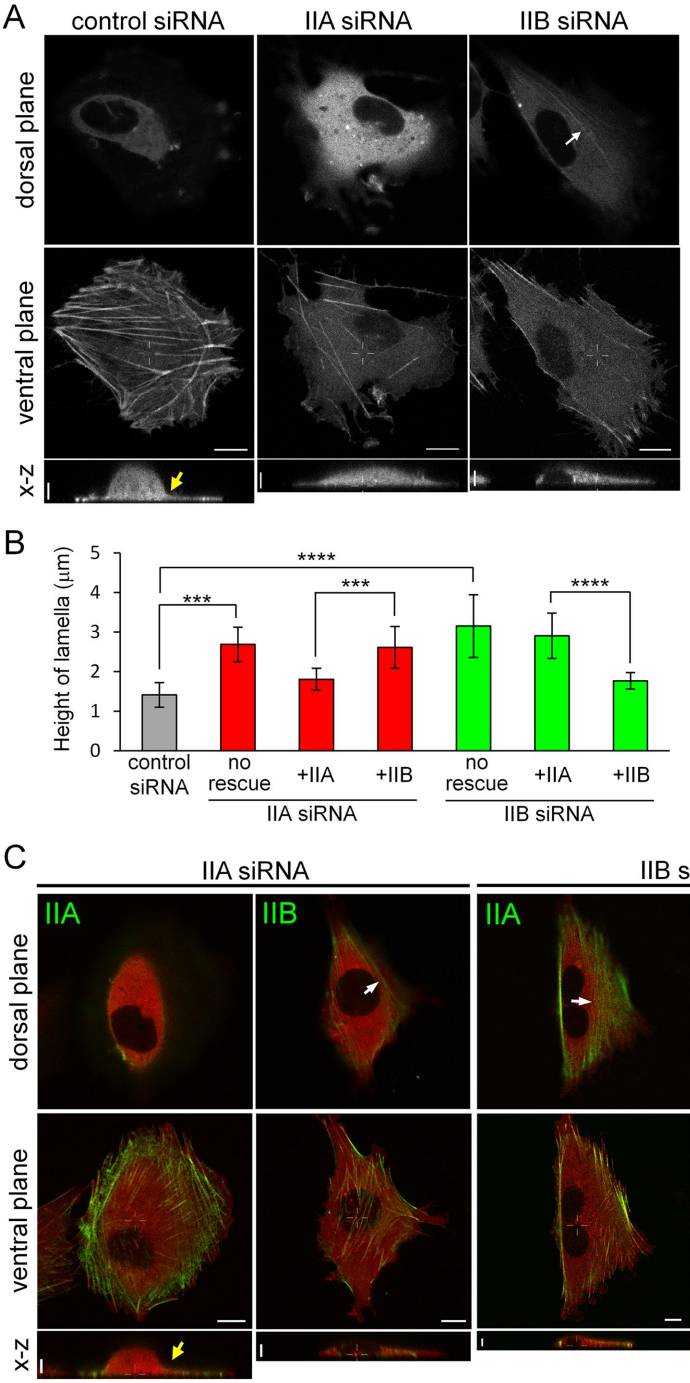

FIGURE 3: Both NMIIA and NMIIB are required for normal lamellar flattening. (A) SV1 cells expressing mCherry-actin were treated with the indicated siRNAs. The dorsal planes are 2 μm above the ventral planes. The white arrow in the dorsal plane of the NMIIB-KD cell points to a remaining TA. Side views are *x*–*z* maximum intensity projections of the white lines in each ventral plane. The yellow arrow in the side view of the control siRNA-treated cell indicates the boundary between the lamella and cell body. Note that this boundary was clear in the control cell but not in NMIIA-KD and NMIIB-KD cells. (B) Height of lamellae in cells in the conditions shown in A and C. The portion corresponding to the lamella was defined as that between the highest portion of the cell body and the extending edge of the cell in the side view, and its height was measured using ImageJ software. Data represent the mean ± SD from $n > 8$ cells. ***$p < 0.0005$, ****$p < 0.00005$. (C) Rescue experiments of the lamellar flattening defect in NMIIA-KD and NMIIB-KD cells on exogenous expression of each NMII isoform. SV1 cells treated with the indicated siRNAs were transfected with the indicated siRNA-insensitive EGFP-NMHC-II isoform and mCherry-actin. White arrows in the dorsal planes point to TAs. Yellow arrows in the side views indicate the boundary between the lamella and cell body. Note that this boundary is clear in NMIIA-KD and NMIIB-KD cells expressing exogenous NMIIA and NMIIB, respectively. Also note that exogenously expressed NMIIB localized to the distal region of the lamella in NMIIA-KD cells, but not in NMIIB-KD cells. All live cell images were captured using a confocal microscope. *x*–*y* views: bar, 10 μm. *x*–*z* views: bar, 5 μm.

et al., 2016; Hu *et al.*, 2017; Titus, 2017). Immunofluorescence staining of NMIIA showed periodic lines emanating from the stacks of NMII filament spots in the distal or proximal region of lamellae (Figure 4A). The distance between the stacks of NMII filaments was decreased in control cells (Figure 4, B and C). Moreover, TAs became less curved during centripetal flow (Supplemental Movies S2 and S5). These results indicate that the length of TAs was shortened by contraction. However, there was no change in the distance between the stacks of NMII filaments in NMIIB-KD cells during centripetal flow (Figure 4, A–C), suggesting that the defect in lamellar flattening in these cells is due to the inability of TAs to contract.

Next, to determine the significance of each NMII isoform in proper contraction of TAs, we measured the distances between NMII filaments in cells treated with each siRNA and expressing exogenous EGFP-NMHC-IIA or EGFP-NMHC-IIB (Figure 4C). The distance between NMII filaments in NMIIA-KD and NMIIB-KD cells decreased to a level comparable to that in control cells on exogenous expression of EGFP-NMHC-IIA and EGFP-NMHC-IIB, respectively. On the other hand, it was not decreased in NMIIA-KD and NMIIB-KD cells expressing exogenous EGFP-NMHC-IIB and EGFP-NMHC-IIA, respectively. In summary, the contraction defects were not rescued by expression of the other isoform. These results indicate that TAs containing only NMIIA or NMIIB are unable to contract properly. Both isoforms are required for the normal contraction of TAs during lamellar flattening (Figure 4D).

Actin filaments in vSFs are in a stretched conformation

Actin filaments undergo conformational changes to function as a tension sensor (Uyeda *et al.*, 2011; Hayakawa *et al.*, 2011; Galkin *et al.*, 2012; Burridge and Guilluy, 2016). Uyeda *et al.* (2011) reported that the myosin II motor domain subfragment 1 (S1) can bind to actin filaments localizing in stretched regions of *Dictyostelium discoideum* cells. Tang and Ostap (2001) reported that S1 of NMIIB can bind to selected SFs in mammalian cells. These reports prompted us to investigate stretch-induced

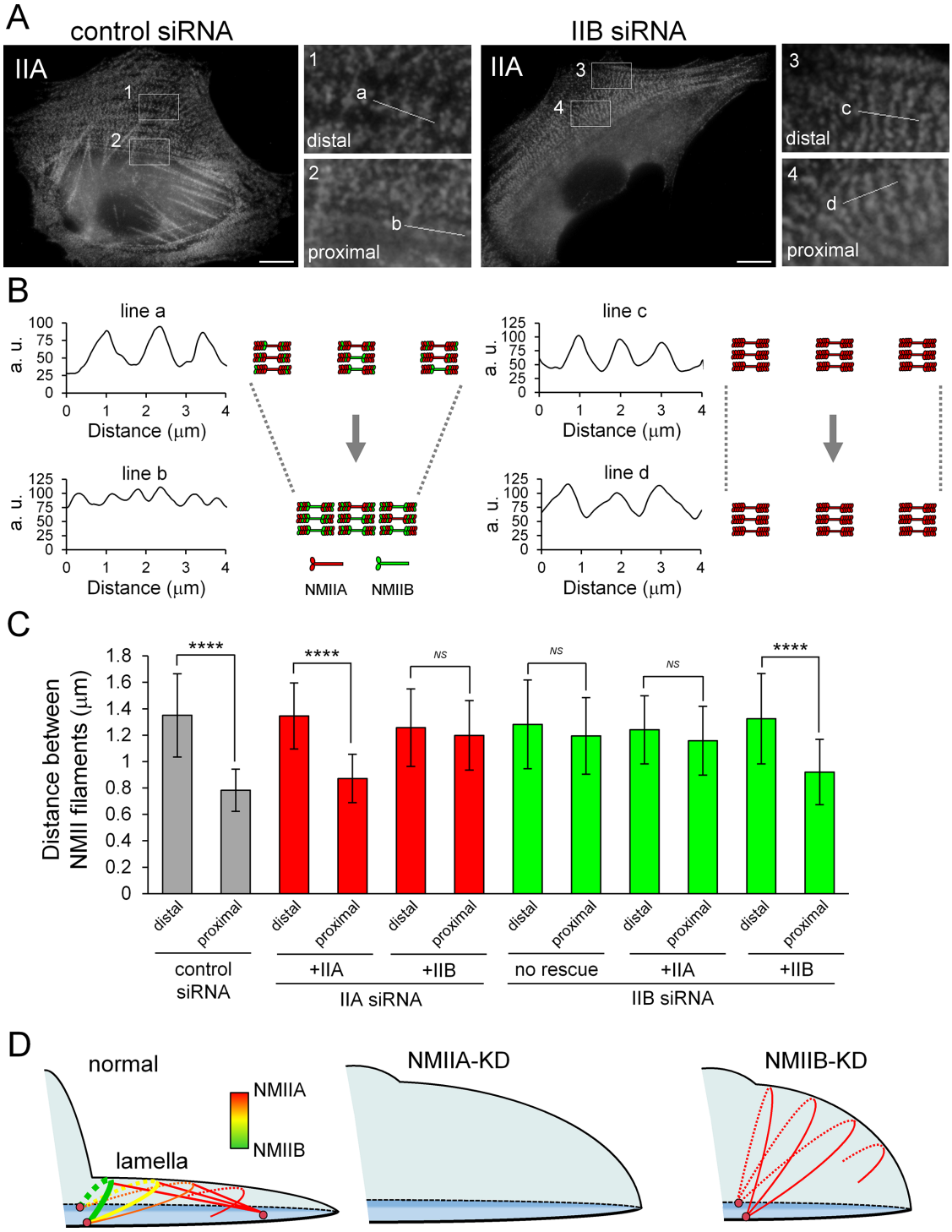

FIGURE 4: Both NMIIA and NMIIB are required for normal contraction of TAs. (A) SV1 cells treated with the indicated siRNAs were fixed and stained with an Alexa Fluor 596–conjugated anti–NMHC-IIA polyclonal antibody. Enlarged images of the boxed regions in the overall image showing the central portion of TAs. Images were captured using a conventional fluorescence microscope. Bar, 10 μm. (B) Scans along the white lines in A showing the distances between the stacks of NMII filaments in TAs. The schematic illustrations indicate the contraction process of TAs in each condition. (C) Quantification of the distance between NMII filaments in each condition ($n > 30$ pitches from >5 cells/condition). The distances between NMII filaments were measured by the RGB Profile plot plug-in of ImageJ software. ****$p < 0.00005$. Note that the distance between stacks was not decreased in NMIIB-KD cells during centripetal flow. (D) Model for the role of TAs in lamellar flattening. Schematic illustration depicting the lamellar shape of each siRNA-treated cell. Arcs, straight lines, and pink circles indicate TAs, dSFs connecting to TAs at right angles, and FAs, respectively. Red and green correspond to NMIIA and NMIIB in the SF subtypes, respectively. TAs form via the association of NMIIA with actin filaments in the distal region of the lamella and are then transferred to the cell body. During centripetal flow, TAs link to FAs derived from the distal end of dSFs at both ends (Hotulainen and Lappalainen, 2006), as well as to dSFs connecting

conformational differences of actin filaments in each SF subtype by examining NMIIB-S1 binding. In *Dictyostelium* cells, S1 mutants with a high affinity for actin filaments bind to stretched actin filaments in the presence of physiological ATP concentrations (Uyeda *et al.*, 2011). Thus, we examined the cellular localizations of several S1 mutants to identify the best probe for actin filaments in selected SFs. The N93K and R702C mutations in human NMHC-IIA, which are associated with certain genetic disorders, inhibit actin-activated Mg^{2+}-ATPase activity and actin filament translocation in vitro (Hu *et al.*, 2002). N97K and R709C in human NMHC-IIB are artificial mutations that correspond to N93K and R702C in NMHC-IIA, respectively (Kim, Kovács, *et al.*, 2005). We prepared S1-EGFP constructs containing one of these mutations, in addition to the wild type, and performed live cell imaging of S1-EGFP-expressing cells to avoid possible artifacts caused by fixation and permeabilization during immunofluorescence staining. None of the NMIIA-S1 constructs localized to SFs (unpublished data). Among the NMIIB-S1 constructs, only NMIIB-S1-R709C-EGFP clearly localized to specific SFs, and a pool of it remained in the Triton-insoluble fraction (Supplemental Figure S7). The organization of SF subtypes was not affected by expression of NMIIB-S1-R709C-EGFP. Thus, this mutant is unlikely to prevent the binding of endogenous NMII to F-actin. NMIIB-R709C heavy meromyosin displays very slow ADP release, indicating that it is predominantly in a strong actin-binding state during the ATPase cycle (Kim and Kovács, *et al.*, 2005). This inherent property of the R709C mutant might be useful to detect distinct SFs with a higher affinity for the motor domain of NMIIB.

To determine whether NMIIB-S1-R709C-EGFP recognizes a specific conformational feature of stretched actin filaments, we stretched cells using a stretch device. We measured the fluorescence intensity of NMIIB-S1-R709C-EGFP in SFs before and after stretching and normalized it with respect to that of mCherry-actin. Figure 5A shows SV1 cells expressing NMIIB-S1-R709C-EGFP and mCherry-actin before and after 14% stretching. Cell stretching increased the relative fluorescence intensity of EGFP, indicating that it promoted binding of NMIIB-S1-R709C to SFs (Figure 5, B and C). These results suggest that NMIIB-S1-R709C can recognize a conformational change of actin filaments and preferentially binds to stretched actin filaments. Therefore, we selected NMIIB-S1-R709C-EGFP as a probe for stretched actin filaments in SFs.

To observe the behavior of NMIIB-S1-R709C-EGFP in live cells, we acquired time-lapse images of SV1 cells expressing this probe and mCherry-actin. NMIIB-S1-R709C-EGFP was observed in less-mobile vSFs but not in mobile TAs (Supplemental Movie S13 and Figure 5, D and E). We next investigated the involvement of each NMII isoform in the different F-actin conformational states (Figure 6, A and B). In control cells, NMIIB-S1-R709C clearly localized along straight SFs, such as vSFs. In NMIIA-KD cells, binding of NMIIB-S1-R709C-EGFP to the remaining vSFs was decreased, demonstrating that actin filaments in vSFs lacking NMIIA are not highly stretched. However, we cannot conclude whether the decrease in S1 binding is due to the loss of total NMII molecules or the reduction in NMIIA-specific motor activity. Owing to the loss of vSFs in NMIIB-KD cells, we were unable to determine whether NMIIB-S1-R709C-EGFP localizes along vSFs in the absence of NMIIB. NMIIB-S1-R709C-EGFP weakly localized to both ends of relatively straight TAs in lamellae of NMIIB-KD cells. Taken together, these results suggest that actin filaments in straight SFs, such as less mobile vSFs, are in a stretched conformation, whereas those in mobile TAs are not (Figure 6C).

DISCUSSION

In this study, we found that NMIIA and NMIIB are required for the formation of TAs and vSFs in fibroblasts, respectively. Moreover, we demonstrated that both isoforms are necessary for the proper organization and function of each SF subtype.

SFs are dynamic structures that are organized in a spatiotemporally regulated manner in cells, and the turnover of NMII by assembly/disassembly of filaments is important for this organization (Vicente-Manzanares *et al.*, 2009; Heissler and Manstein, 2013; Beach and Hammer, 2015). TAs form at the interface between lamellipodia and lamella (Hotulainen and Lappalainen, 2006; Burnette *et al.*, 2011). NMIIA filaments are turned over more rapidly than NMIIB filaments in cells, and, consequently, NMIIA arrives at newly formed lamellae prior to NMIIB (Kolega, 1998; Sandquist and Means, 2008; Vicente-Manzanares *et al.*, 2008). This is consistent with the notion that NMIIA is involved in the formation of TAs (Figure 2) (Burnette *et al.*, 2011, 2014; Beach *et al.*, 2017). The expression level of NMIIB is only about 1/15th that of NMIIA in SV1 cells (Sato *et al.*, 2007). Therefore, the low level of remaining NMIIB molecules in NMIIA-KD cells might prevent delivery of this isoform to the distal region of the lamella; most molecules would form vSFs in the cell body. Exogenously expressed NMIIB rescued the formation of TAs in NMIIA-KD cells (Figure 2 and Supplemental Figure S5). However, excess exogenous NMIIB did not localize to the distal region of the lamella in NMIIB-KD cells, in which endogenous NMIIA was expressed (Figure 3C and Supplemental Figure S5). We speculate that excess exogenous NMIIB can reach the distal region of the lamella and form TAs in this region when endogenous NMIIA, which normally forms nascent TAs and occupies the position of NMIIs in those TAs, is depleted. Therefore, regarding the formation of TAs, NMIIB can functionally compensate for the loss of NMIIA if it can reach the region where nascent TAs form.

A distinctive morphological feature of the lamella is its extremely thin and flattened shape. Burnette *et al.* (2014) proposed that mechanical coupling exists between TAs and dSFs and that TA contractility generates the force needed to pull dSFs inward and to flatten lamellae. They showed that the flattened shape of lamellae is not maintained in COS-7 cells (NMIIA-null) and NMIIA-KD U-2 OS cells and that this defect is rescued by exogenous expression of NMIIA. On the basis of these findings, they proposed that NMIIA is indispensable for lamellar flattening. In this study, we found that NMIIB-KD cells lacked flattened lamellae, even though TAs, which consisted only of NMIIA, formed (Figure 3). TAs consisting only of NMIIB, which formed in NMIIA-KD cells expressing excess exogenous NMIIB, were also unable to flatten the lamella. We speculate that loss of TA contractility (Figure 4) is the main cause of the lamellar flattening defect. To maintain the uniformly thin and flattened shape of the lamella, a greater contractile force may be required in the proximal region than in the distal region due to the thickness of the cell body. NMIIB predominantly localizes to proximal TAs, whereas NMIIA localizes along all TAs in U-2 OS cells (Vallenius, 2013; Beach *et al.*, 2014) and SV1 cells (Figure 1). It was recently demonstrated

to TAs at right angles, and then NMIIB is incorporated into TAs. TAs do not form in NMIIA-KD cells. The flattened lamella is maintained by the contraction of TAs. The tension generated by this contraction is transmitted to FAs at the distal end of dSFs (Burnette *et al.*, 2014). Thus, lamellar flattening is affected in both NMIIA-KD and NMIIB-KD cells due to the lack of TAs and the absence of functional TAs, respectively.

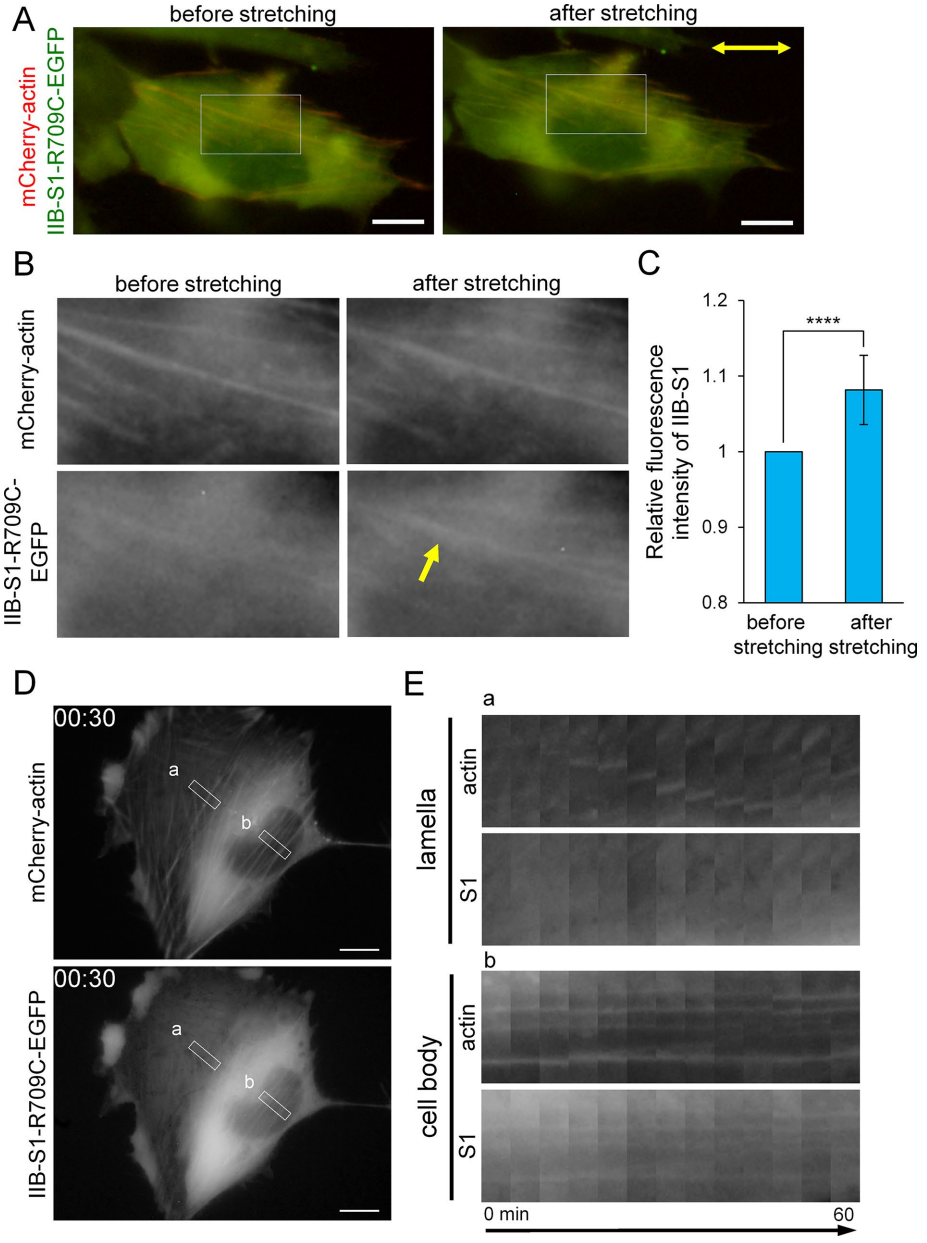

FIGURE 5: NMIIB-S1-R709C-EGFP can be used as a probe for stretched actin filaments. (A) Images of live SV1 cell expressing NMIIB-S1-R709C-EGFP and mCherry-actin before and after stretching. The silicone chamber was stretched by 14% in the direction indicated by the two-way arrow. (B) Enlarged images of the boxed regions in A showing some SFs. The yellow arrow indicates a representative SF in which the fluorescence intensity of NMIIB-S1-R709C-EGFP was increased after stretching. (C) Fluorescence intensities of NMIIB-S1-R709C-EGFP in the control and SF areas were quantified using the RGB Measure plug-in of ImageJ software. The relative fluorescence intensity of NMIIB-S1-R709C-EGFP in the SF area versus the control area was calculated for each image and normalized by that of mCherry-actin. Data represent the mean ± SD from nine independent experiments. ****$p < 0.00005$. (D) Still images showing mCherry-actin and NMIIB-S1-R709C-EGFP fluorescence from Supplemental Movie S13 at 30 min. (E) Kymographs generated from the boxed regions in D. Boxes a and b indicate the regions containing TAs in the lamella and vSFs in the cell body, respectively. Note that NMIIB-S1-R709C-EGFP bound to less mobile vSFs, but not to mobile TAs. All images were captured using a conventional fluorescence microscope. Bar, 10 μm.

that NMIIA and NMIIB coassemble into heterofilaments in cells (Beach *et al.*, 2014; Shutova *et al.*, 2014). The incorporation of NMIIB into preformed filaments consisting of NMIIA during centripetal flow was directly observed by live cell imaging using superresolution microscopy (Beach *et al.*, 2014). Although the underlying molecular mechanism that explains why both NMIIA and NMIIB are required for lamellar flattening is unclear, we speculate that TAs might be able to generate tension via the incorporation of NMIIB into preformed NMIIA filaments. NMIIB is a relatively high duty ratio motor (Rosenfeld *et al.*, 2003; Wang, Kovács, *et al.*, 2003). Moreover, the ADP release rate of both isoforms, especially NMIIB, is decreased by the resisting load, suggesting that NMIIB plays a role in the maintenance of tension (Kovács *et al.*, 2007). In addition to the high motor activity of NMIIA, this unique property of NMIIB (tension-bearing role) might help to maintain actin filaments in the contracted state in TAs.

Less is known about the organizational properties of vSFs than about those of TAs. In particular, the mechanism via which vSFs form at the ventral surface in the central region of the cell body remains obscure (Small *et al.*, 1998; Skau and Waterman, 2015). It has been proposed that some vSFs are generated via the fusion of TAs with dSFs (Hotulainen and Lappalainen, 2006). Consequently, these vSFs are arch-like structures with their central regions localizing beneath the dorsal surface and both their ends linking to FAs in the ventral surface and orienting parallel to the leading edge (Schulze *et al.*, 2014; Tojkander *et al.*, 2015). However, typical vSFs formed in the central region are unlikely to be generated via this mechanism because their orientation and location differ from those of vSFs formed from TAs and dSFs. Beach *et al.* (2017) recently observed the formation of TAs and typical vSFs simultaneously using superresolution 3D microscopy. Their findings suggest that typical vSFs do not form via the fusion of TAs with dSFs. Thus, hereafter we refer to typical vSFs simply as vSFs. vSFs can form in COS-7 cells (Bao *et al.*, 2005; Burnette *et al.*, 2014) and NMIIA-KD SV1 cells (Figure 2). Moreover, vSFs almost completely disappeared in NMIIB-KD cells and exogenous expression of NMIIA failed to rescue this defect (Figure 2). The disappearance of SFs and FAs from the central region of the cell body on NMIIB KD has been reported in other cell types (Sandquist *et al.*, 2006; Betapudi, 2010; Jorrisch *et al.*, 2013). Thus, it is assumed that NMIIB is indispensable for the organization of vSFs and that NMIIA cannot replace the function of NMIIB in this context. The unique tension-bearing role of NMIIB might be necessary for the organization of vSFs.

In addition to their mechanisms of formation, the dynamics of vSFs and TAs also significantly differ. TAs can shorten in length

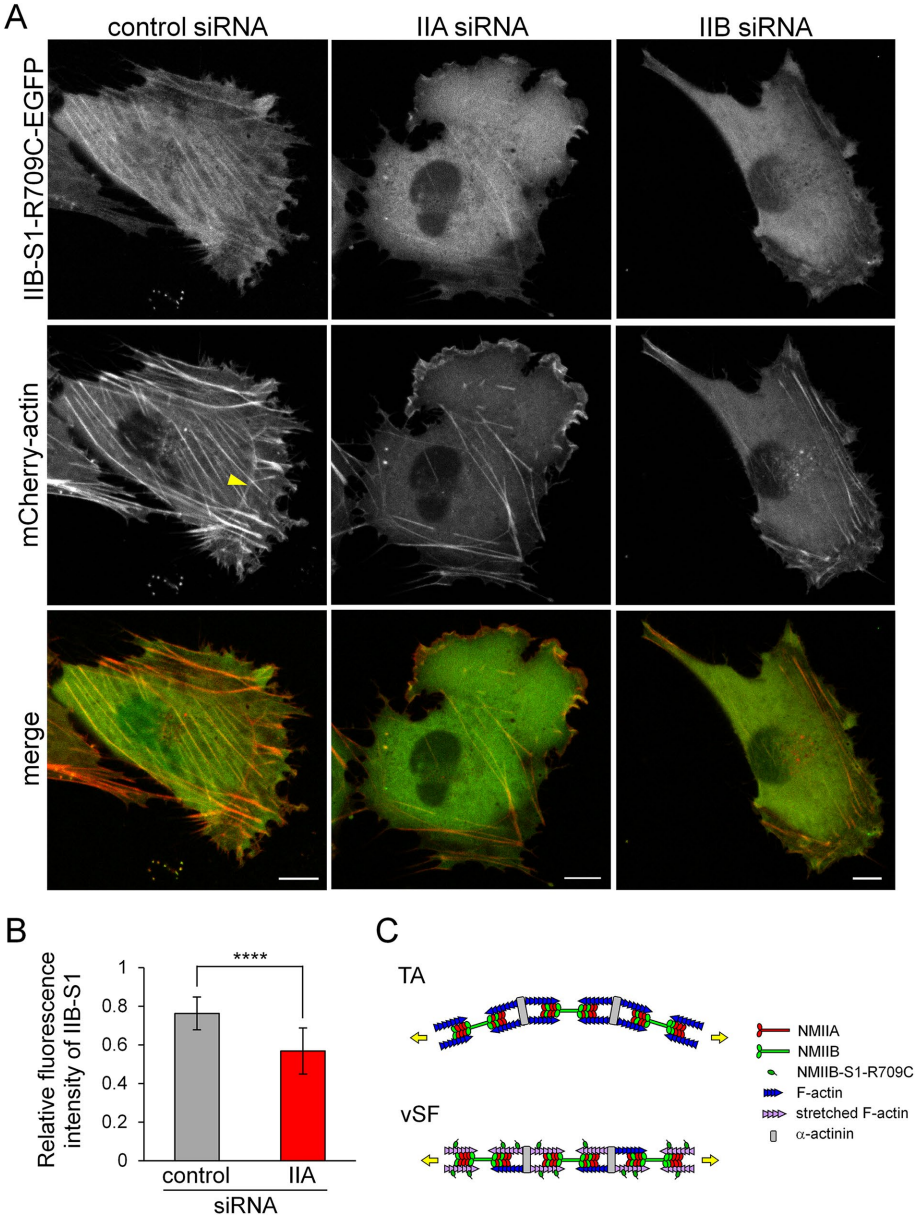

FIGURE 6: Both NMIIA and NMIIB are required for the normal organization of vSFs. (A) SV1 cells treated with the indicated siRNAs were transfected with siRNA-insensitive NMIIB-S1-R709C-EGFP and mCherry-actin. Live cell images were captured using a confocal microscope. Bar, 10 μm. The yellow arrowhead points to a curved TA. Note that NMIIB-S1-R709C-EGFP did not bind to curved TAs. The fluorescence intensity of NMIIB-S1-R709C-EGFP relative to that of mCherry-actin in vSFs was lower in NMIIA-KD cells than in control cells. (B) The ratio of the fluorescence intensity of NMIIB-S1-R709C-EGFP to that of mCherry-actin in vSFs in control and NMIIA-KD cells. The relative fluorescence intensity of NMIIB-S1-R709C-EGFP in the SF area versus the control area was quantified and normalized by that of mCherry-actin using the RGB Measure plug-in of ImageJ software. Data represent the mean ± SD from $n = 25$ SFs from five cells. ****$p < 0.00005$. (C) Schematic model of the organization of SF subtypes. The key difference between TAs and vSFs is their contraction mode. Specifically, vSFs undergo isometric contraction (length remains constant), whereas TAs are shortened during centripetal flow. Therefore, if an equal load is applied to these structures, vSFs generate greater tension than TAs, resulting in the stretching of actin filaments, which is recognized by NMIIB-S1-R709C.

during centripetal flow, probably because they have a curved shape. By contrast, the length of vSFs remains constant, in association with their less dynamic movement, because they are linked to FAs at both ends and have a straight shape (Figure 1). Therefore, tension would be high in vSFs in the so-called isometric contraction state (Deguchi and Sato, 2009; Kassianidou and Kumar, 2015). In this study, we showed that NMIIB-S1-R709C-EGFP (hereafter referred to as the S1 probe) bound to relatively straight SFs such as vSFs (Figures 5 and 6). This binding was increased by external stretching of cells (Figure 5). Moreover, binding of the S1 probe was evaluated by assessing its fluorescence intensity after normalization against that of mCherry-actin; therefore, the increase in the binding of this probe was not due to the increase in the density of actin filaments in SFs. Certain actin filament-binding proteins, such as tropomyosin isoforms, can bind to different SF subtypes in an isoform-dependent manner (Bryce *et al.*, 2003; Tojkander *et al.*, 2011; Gateva *et al.*, 2017). Although we cannot exclude the possibility that binding of these proteins mediates the preferential binding of the S1 probe to stretched actin filaments, we conclude that this probe can recognize certain qualitative changes of stretched actin filaments in loaded SFs. Traction force microscopy, which images displacement of a substrate by cells, revealed that NMIIA-KD cells cannot generate proper traction force (Jorrisch *et al.*, 2013; Chang and Kumar, 2015; Thomas *et al.*, 2015). This correlates well with our finding that binding of the S1 probe to vSFs was decreased in NMIIA-KD cells (Figure 6). The S1 probe is a valuable tool to directly distinguish stretched SFs in mechanobiology studies.

During the revision of this article, a related paper was published, which reports that NMIIA and NMIIB favor formation of TAs and vSFs, respectively (Shutova *et al.*, 2017). The authors demonstrated that the expression ratio between NMIIA and NMIIB is important for the organization of SF subtypes. Specifically, TAs and vSFs predominantly form in NMIIA-enriched and NMIIB-enriched cells, respectively. They also showed that NMIIA can accelerate NMIIB dynamics in SFs by forming heterofilaments. Consequently, the localization of NMIIB is dependent on the expression level of NMIIA in REF52 and COS-7 cells; NMIIB localizes to the distal region of the lamella and forms TAs in cells expressing a high level of NMIIA but not in cells lacking NMIIA. By contrast, exogenous NMIIB localized in the distal region of the lamella and formed TAs in NMIIA-KD SV1 cells (Supplemental Figure S5). In the other case, we recently found that NMIIB localizes to the posterior region in the migrating TIG-1 cells (human normal fibroblasts that have a polarized shape during migration) and that exogenously expressed NMIIB is still restricted to the posterior region in the NMIIA-KD cells

(Kuragano *et al.*, unpublished data). These differences in the behavior of NMIIB might be due to differences in intracellular signaling pathways between the cell lines.

In this study, we referred to arch-like SFs, which formed via the fusion of TAs with dSFs in the proximal region of the lamella, as TAs rather than vSFs based on the localization of their central portion at the dorsal surface (Burnette *et al.*, 2014; Schulze *et al.*, 2014) and their function in lamellar flattening. However, this terminology may be confusing because the ends of these SFs link to FAs, which could be derived from dSFs (Hotulainen and Lappalainen, 2006). Consequently, this SF may need to be renamed in the future. In conclusion, our results revealed that NMIIA and NMIIB are required for the formation of TAs and vSFs, respectively, and that the presence of both isoforms in TAs is required to maintain the thin and flattened shape of the lamella. We also raised the possibility that actin filaments in straight SFs, such as vSFs, are in a stretched conformation that is distinct from that of other actin filaments in the same cells. It should be noted that KD of NMIIB significantly affects the organization of SF subtypes even though its expression level is much lower than that of NMIIA. NMIIB would maintain the contraction state of the actomyosin structure, which is hardly performed by NMIIA.

MATERIALS AND METHODS

Cell culture

MRC-5 SV1 TG1 cells (cell no. RCB0207; SV40-transformed MRC-5 human embryonic lung fibroblasts) were obtained from the RIKEN Cell Bank (Tsukuba, Japan) and maintained in MEM alpha (Life Technologies, Carlsbad, CA) supplemented with 10% fetal bovine serum (FBS) (BioSource/Life Technologies), 50 U/ml penicillin, and 50 μg/ml streptomycin (Life Technologies). Cells were cultured at 37°C in humidified air containing 5% CO_2. The cell line was authenticated by short tandem repeat analysis (Takara Bio, Kusatsu, Japan). Cells were routinely tested for mycoplasma contamination by DAPI (4′,6-diamidino-2-phenylindole) staining.

Antibodies and reagents

Anti–NMHC-IIB and anti–NMHC-IIA polyclonal antibodies targeting the carboxyl terminus of NMHC-IIB and NMHC-IIA, respectively, were used as previously described (Saitoh *et al.*, 2001; Sato *et al.*, 2007). An anti-vinculin monoclonal antibody (hVIN-1) and FITC-conjugated phalloidin were purchased from Sigma-Aldrich (St. Louis, MO). Alexa Fluor 350–labeled phalloidin was purchased from Molecular Probes (Eugene, OR). Cy3-conjugated goat anti-rabbit immunoglobulin G (IgG) (H+L) and Cy3-conjugated goat anti-mouse IgG (H+L) were purchased from Jackson ImmunoResearch Laboratories (West Grove, PA). Fibronectin purified from human plasma was purchased from Roche Diagnostics (Basel, Switzerland).

Plasmids

pEGFP-C1 was purchased from Takara Bio USA (formerly Clontech Laboratories, Mountain View, CA). pEGFP-vinculin (plasmid no. 50513) was purchased from Addgene (Cambridge, MA). pEGFP-NMHC-IIB (Wei and Adelstein, 2000) was a kind gift from. Robert S. Adelstein (National Institutes of Health [NIH], Bethesda, MD). pmCherry-NMHC-IIA was prepared as previously described (Kiboku *et al.*, 2013). pEGFP-NMHC-IIA* and pEGFP-NMHC-IIB*, which encode the siRNA-insensitive forms of NMHC-IIA and NMHC-IIB, respectively, were generated via a two-step process. First, the fragments obtained by restriction digestion of pEGFP-NMHC-IIA with *Eco*RI-*Sal*I and pEGFP-NMHC-IIB with *Eco*RI were subcloned into pBluescript II SK$^+$ (Stratagene, La Jolla, CA). Fragments of NMHC-IIA and NMHC-IIB harboring siRNA-insensitive mutations were generated by inverse PCR using pBluescript II SK$^+$ containing the respective fragments as templates and the primers listed in Supplemental Table S1. Next, these plasmids containing fragments of NMHC-IIA and NMHC-IIB with siRNA-insensitive sequences were digested with *Eco*RI-*Sal*I and *Eco*RI, respectively, and the digestion products were subcloned into the same sites of pEGFP-NMHC-IIA-WT and pEGFP-NMHC-IIB-WT, respectively. pmCherry-actin was prepared as previously described (Kondo *et al.*, 2011) using mCherry cDNA (Shaner *et al.*, 2004). The regions encoding S1, which contained the motor domain and the lever arm, of NMHC-IIB and NMHC-IIA were amplified by PCR using pEGFP-NMHC-IIB and pEGFP-NMHC-IIA as templates, respectively, and the primer pairs listed in Supplemental Table S1. The PCR products encoding NMIIB-S1 and NMIIA-S1 were subcloned into the *Bgl*II-*Kpn*I and *Hin*dIII-*Kpn*I sites of pEGFP-N3 (Takara Bio USA) to generate pNMIIB-S1-EGFP and pNMIIA-S1-EGFP, respectively. Plasmids encoding NMIIB-S1 and NMIIA-S1 point mutants were generated by inverse PCR using pNMIIB-S1-EGFP and pNMIIA-S1-EGFP as templates, respectively. pNMIIB*-S1-R709C-EGFP, which encodes the siRNA-insensitive form of NMIIB-S1-R709C, was generated by inverse PCR using pNMIIB-S1-R709C-EGFP as a template and the primers listed in Supplemental Table S1. The nucleotide sequences of the DNA fragments amplified by PCR were verified by sequencing using an ABI PRISM 310 DNA sequencer (Applied Biosystems, Foster City, CA).

Immunofluorescence

Cells were fixed with 3.7% formaldehyde prepared in phosphate-buffered saline (PBS) for 15 min and permeabilized with 0.1% Triton X-100 prepared in PBS for 10 min. Fixed cells were preincubated with blocking solution (3% bovine serum albumin [BSA] prepared in PBS) for 30 min. Thereafter, cells were incubated with primary antibodies diluted in blocking solution for 60 min, washed three times with PBS, incubated with the appropriate secondary antibodies diluted in blocking solution for 60 min, and subsequently washed three times with PBS. To stain actin filaments, Alexa Fluor 350– or FITC-conjugated phalloidin (0.5 μg/ml) was added to the secondary antibody solution. The antibodies used for indirect immunofluorescence were as follows: anti-vinculin monoclonal antibody (1:5000) and Cy3-conjugated goat anti-mouse IgG (H+L) (1:500). For direct immunofluorescence, the antibodies were labeled with Alexa Fluor 488 or Alexa Fluor 596 using the Zenon Antibody Labeling Kit (Molecular Probes) according to the manufacturer's protocol. To simultaneously stain NMHC-IIB and NMHC-IIA, samples were incubated with Alexa Fluor 596–conjugated anti–NMHC-IIA (1:2000) and Alexa Fluor 488–conjugated anti–NMHC-IIB (1:2000) antibodies for 60 min. Thereafter, cells were fixed with 3.7% formaldehyde prepared in PBS for 15 min and incubated with Alexa Fluor 350–labeled phalloidin (0.5 μg/ml) for 60 min. Images were captured using a conventional fluorescence microscope (BX50WI; Olympus, Tokyo, Japan) equipped with a single-chip color charge-coupled device (CCD) camera (DP70; Olympus) and an objective lens (UPlanApo 60×/0.90 NA; UPlanFl 100×/1.30 NA Oil; Olympus) together with DP Controller software (Olympus). All procedures were performed at room temperature. Immunofluorescence images were analyzed using ImageJ software (NIH, Bethesda, MD).

Transfection

Cells were transfected with plasmid DNA using Xfect Transfection Reagent (Takara Bio USA) in FBS-free and antibiotic-free OPTI-MEM (Life Technologies) according to the manufacturer's protocol. After incubation for 1 h under standard culture conditions, cells were

replated onto coverslips (Matsunami, Kishiwada, Japan) or glass-bottom dishes (IWAKI, ASAHI GLASS, Tokyo, Japan) precoated with 10 µg/ml fibronectin for immunofluorescence or time-lapse observation, respectively.

Time-lapse observation

Time-lapse images were captured with an inverted microscope (IX71; Olympus) equipped with a single-chip color CCD camera (DP70; Olympus) and an objective lens (UPlanFl 100×/1.30 NA Oil; Olympus). During observation, cells were maintained in DMEM/F12 (1:1) (Life Technologies) supplemented with 10% FBS and warmed on a thermoplate set to 37°C (MATS-U55R30; Tokai Hit, Fujinomiya, Japan). Images were captured every 5 min and analyzed using DP Controller software (Olympus).

Confocal laser scanning microscopy

Live cell images were captured using an inverted microscope (Ti-E; Nikon, Tokyo, Japan) and a confocal laser microscope system (A1R; Nikon) equipped with an oil-immersion objective lens (Plan Apo VC 60×/1.40 NA Oil; Nikon). Cells were maintained in DMEM/F12 (1:1) (Life Technologies) supplemented with 10% FBS and warmed in a chamber set to 37°C (INUBG2H-TIZB; Tokai Hit) during observation. Z-stack images were oversampled by taking z-steps of 230 nm between acquired images. Images were captured and analyzed using NIS-Elements C software (Nikon).

KD of NMHC-IIA and NMHC-IIB

Human NMHC-IIA–specific (GGCCAAAGAGAACGAGAAGUU), human NMHC-IIB–specific (GGAUCGCUACUAUUCAGGAUU), and nonsense (GCGCGCUUUGUAGGAUUCGUU) siRNAs were purchased from Thermo Scientific Dharmacon (Waltham, MA). A total of 2×10^4 cells were transfected with 20 pmol of each siRNA using Lipofectamine RNAiMAX Transfection Reagent (Invitrogen) in a 24-well plate according to the manufacturer's protocol. After transfection for 72 h, immunofluorescence or time-lapse observation was performed. To express exogenous proteins, cells were transfected with the respective expression vector at 24 h after siRNA transfection.

Cell stretching

A stretch device was constructed using the universal plate set (No. 98; TAMIYA, Shizuoka, Japan) as a base board. The plate was equipped with a silicone soft mold (Plate G; Kameshima Co., Ltd., Osaka, Japan) as a cell culture chamber. One edge of the silicone chamber was fixed to an immobile bar attached to the plate, and the opposite edge was connected to a movable bar for stretching. SV1 cells expressing NMIIB-S1-R709C-EGFP and mCherry-actin were plated on the silicon chamber precoated with 50 µg/ml fibronectin. During observation, cells were maintained in DMEM/F12 (1:1) (Life Technologies) supplemented with 10% FBS at 25°C. Live cell images were captured using a conventional fluorescence microscope (BX50WI; Olympus) equipped with a single-chip color CCD camera (DP70; Olympus) and a water immersion objective lens (LUMPlanFl 60×/0.90 NA; Olympus).

ACKNOWLEDGMENTS

We are grateful to the Nikon Imaging Center (Hokkaido University) for assistance with microscopy, image acquisition, and analysis. We are also grateful to Hisashi Haga (Hokkaido University) and Takeomi Mizutani (Hokkai-Gakuen University, Sapporo, Japan) for helpful advice on the cell stretching assay. This work was supported by Grants-in-Aid for Scientific Research from the Japan Society for the Promotion of Science (JSPS) (no. 25440061 to M.T.). Part of this work was supported by the "Nanotechnology Platform" Program of the Ministry of Education, Culture, Sports, Science, and Technology (MEXT), Japan, and also by JSPS KAKENHI Grant Number JP16H06280, a Grant-in-Aid for Scientific Research on Innovative Areas-Resource, and technical support platforms for promoting research "Advanced Bioimaging Support."

REFERENCES

Boldface names denote co–first authors.

Bao J, Jana SS, Adelstein RS (2005). Vertebrate nonmuscle myosin II isoforms rescue small interfering RNA-induced defects in COS-7 cell cytokinesis. J Biol Chem 280, 19594–19599.

Beach JR, Bruun KS, Shao L, Li D, Swider Z, Remmert K, Zhang Y, Conti MA, Adelstein RS, Rusan NM, *et al*. (2017). Actin dynamics and competition for myosin monomer govern the sequential amplification of myosin filaments. Nat Cell Biol 19, 85–93.

Beach JR, Hammer JA (2015). Myosin II isoform co-assembly and differential regulation in mammalian systems. Exp Cell Res 334, 2–9.

Beach JR, Shao L, Remmert K, Li D, Betzig E, Hammer JA III (2014). Nonmuscle myosin II isoforms coassemble in living cells. Curr Biol 24, 1160–1166.

Betapudi V (2010). Myosin II motor proteins with different functions determine the fate of lamellipodia extension during cell spreading. PLoS One 5, e8560.

Betapudi V, Licate LS, Egelhoff TT (2006). Distinct roles of nonmuscle myosin II isoforms in the regulation of MDA-MB-231 breast cancer cell spreading and migration. Cancer Res 66, 4725–4733.

Bryce NS, Schevzov G, Ferguson V, Percival JM, Lin JJ-C, Matsumura F, Bamburg JR, Jeffrey PL, Hardeman EC, Gunning P, Weinberger RP (2003). Specification of actin filament function and molecular composition by tropomyosin isoforms. Mol Biol Cell 14, 1002–1016.

Burnette DT, Manley S, Sengupta P, Sougrat R, Davidson MW, Kachar B, Lippincott-Schwartz J (2011). A role for actin arcs in the leading-edge advance of migrating cells. Nat Cell Biol 13, 371–381.

Burnette DT, Shao L, Ott C, Pasapera AM, Fischer RS, Baird MA, Der Loughian C, Delanoe-Ayari H, Paszek MJ, Davidson MW, *et al*. (2014). A contractile and counterbalancing adhesion system controls the 3D shape of crawling cells. J Cell Biol 205, 83–96.

Burridge K, Guilluy C (2016). Focal adhesions, stress fibers and mechanical tension. Exp Cell Res 343, 14–20.

Burridge K, Wittchen ES (2013). The tension mounts: stress fibers as force-generating mechanotransducers. J Cell Biol 200, 9–19.

Cai Y, Biais N, Giannone G, Tanase M, Jiang G, Hofman JM, Wiggins CH, Silberzan P, Buguin A, Ladoux B, Sheetz MP (2006). Nonmuscle myosin IIA-dependent force inhibits cell spreading and drives F-actin flow. Biophys J 91, 3907–3920.

Chang C-W, Kumar S (2015). Differential contributions of nonmuscle myosin II isoforms and functional domains to stress fiber mechanics. Sci Rep 5, 13736.

Chrzanowska-Wodnicka M, Burridge K (1996). Rho-stimulated contractility drives the formation of stress fibers and focal adhesions. J Cell Biol 133, 1403–1415.

Conti MA, Adelstein RS (2008). Nonmuscle myosin II moves in new directions. J Cell Sci 121, 11–18.

Deguchi S, Sato M (2009). Biomechanical properties of actin stress fibers of non-motile cells. Biorheology 46, 93–105.

Even-Ram S, Doyle AD, Conti MA, Matsumoto K, Adelstein RS, Yamada KM (2007). Myosin IIA regulates cell motility and actomyosin-microtubule crosstalk. Nat Cell Biol 9, 299–309.

Fenix AM, Taneja N, Buttler CA, Lewis J, Van Engelenburg SB, Ohi R, Burnette DT (2016). Expansion and concatenation of non-muscle myosin IIA filaments drive cellular contractile system formation during interphase and mitosis. Mol Biol Cell 27, 1465–1478.

Galkin VE, Orlova A, Egelman EH (2012). Actin filaments as tension sensors. Curr Biol 22, 96–101.

Gardel ML, Schneider IC, Aratyn-Schaus Y, Waterman CM (2010). Mechanical integration of actin and adhesion dynamics in cell migration. Annu Rev Cell Dev Biol 26, 315–333.

Gateva G, Kremneva E, Reindl T, Kotila T, Kogan K, Gressin L, Gunning PW, Manstein DJ, Michelot A, Lappalainen P (2017). Tropomyosin isoforms specify functionally distinct actin filament populations in vitro. Curr Biol 27, 705–713.

Hayakawa K, Tatsumi H, Sokabe M (2011). Actin filaments function as a tension sensor by tension-dependent binding of cofilin to the filament. J Cell Biol 195, 721–727.
Heath JP (1983). Behaviour and structure of the leading lamella in moving fibroblasts. I. Occurrence and centripetal movement of arc-shaped microfilament bundles beneath the dorsal cell surface. J Cell Sci 60, 331–354.
Heissler SM, Manstein DJ (2013). Nonmuscle myosin-2: mix and match. Cell Mol Life Sci 70, 1–21.
Hotulainen P, Lappalainen P (2006). Stress fibers are generated by two distinct actin assembly mechanisms in motile cells. J Cell Biol 173, 383–394.
Hu A, Wang F, Sellers JR (2002). Mutations in human nonmuscle myosin IIA found in patients with May-Hegglin anomaly and Fechtner syndrome result in impaired enzymatic function. J Biol Chem 277, 46512–46517.
Hu S, Dasbiswas K, Guo Z, Tee Y-H, Thiagarajan V, Hersen P, Chew T-L, Safran SA, Zaidel-Bar R, Bershadsky AD (2017). Long-range self-organization of cytoskeletal myosin II filament stacks. Nat Cell Biol 19, 133–141.
Jorrisch MH, Shih W, Yamada S (2013). Myosin IIA deficient cells migrate efficiently despite reduced traction forces at cell periphery. Biol Open 2, 368–372.
Kassianidou E, Kumar S (2015). A biomechanical perspective on stress fiber structure and function. Biochim Biophys Acta 1853, 3065–3074.
Kiboku T, Katoh T, Nakamura A, Kitamura A, Kinjo M, Murakami Y, Takahashi M (2013). Nonmuscle myosin II folds into a 10S form via two portions of tail for dynamic subcellular localization. Genes Cells 18, 90–109.
Kim K-Y, Kovács M, Kawamoto S, Sellers JR, Adelstein RS (2005). Disease-associated mutations and alternative splicing alter the enzymatic and motile activity of nonmuscle myosins II-B and II-C. J Biol Chem 280, 22769–22775.
Kolega J (1998). Cytoplasmic dynamics of myosin IIA and IIB: spatial "sorting" of isoforms in locomoting cells. J Cell Sci 111, 2085–2095.
Kondo T, Hamao K, Kamijo K, Kimura H, Morita M, Takahashi M, Hosoya H (2011). Enhancement of myosin II/actin turnover at the contractile ring induces slower furrowing in dividing HeLa cells. Biochem J 435, 569–576.
Kovac B, Teo JL, Mäkelä TP, Vallenius T (2013). Assembly of non-contractile dorsal stress fibers requires α-actinin-1 and Rac1 in migrating and spreading cells. J Cell Sci 126, 263–273.
Kovács M, Thirumurugan K, Knight PJ, Sellers JR (2007). Load-dependent mechanism of nonmuscle myosin 2. Proc Natl Acad Sci USA 104, 9994–9999.
Kovács M, Wang F, Hu A, Zhang Y, Sellers JR (2003). Functional divergence of human cytoplasmic myosin II: kinetic characterization of the non-muscle IIA isoform. J Biol Chem 278, 38132–38140.
Lo C-M, Buxton DB, Chua GCH, Dembo M, Adelstein RS, Wang Y-L (2004). Nonmuscle myosin IIb is involved in the guidance of fibroblast migration. Mol Biol Cell 15, 982–989.
Ma X, Adelstein RS (2014). The role of vertebrate nonmuscle Myosin II in development and human disease. Bioarchitecture 4, 88–102.
Maupin P, Phillips CL, Adelstein RS, Pollard TD (1994). Differential localization of myosin-II isozymes in human cultured cells and blood cells. J Cell Sci 107, 3077–3090.
Oakes PW, Beckham Y, Stricker J, Gardel ML (2012). Tension is required but not sufficient for focal adhesion maturation without a stress fiber template. J Cell Biol 196, 363–374.
Rosenfeld SS, Xing J, Chen L-Q, Sweeney HL (2003). Myosin IIb is unconventionally conventional. J Biol Chem 278, 27449–27455.
Rossier OM, Gauthier N, Biais N, Vonnegut W, Fardin M-A, Avigan P, Heller ER, Mathur A, Ghassemi S, Koeckert MS, *et al.* (2010). Force generated by actomyosin contraction builds bridges between adhesive contacts. EMBO J 29, 1055–1068.
Saitoh T, Takemura S, Ueda K, Hosoya H, Nagayama M, Haga H, Kawabata K, Yamagishi A, Takahashi M (2001). Differential localization of non-muscle myosin II isoforms and phosphorylated regulatory light chains in human MRC-5 fibroblasts. FEBS Lett 509, 365–369.
Sandquist JC, Means AR (2008). The C-terminal tail region of nonmuscle myosin II directs isoform-specific distribution in migrating cells. Mol Biol Cell 19, 5156–5167.
Sandquist JC, Swenson KI, DeMali KA, Burridge K, Means AR (2006). Rho kinase differentially regulates phosphorylation of nonmuscle myosin II isoforms A and B during cell rounding and migration. J Biol Chem 281, 35873–35883.
Sato MK, Takahashi M, Yazawa M (2007). Two regions of the tail are necessary for the isoform-specific functions of nonmuscle myosin IIB. Mol Biol Cell 18, 1009–1017.
Schulze N, Graessl M, Blancke Soares A, Geyer M, Dehmelt L, Nalbant P (2014). FHOD1 regulates stress fiber organization by controlling the dynamics of transverse arcs and dorsal fibers. J Cell Sci 127, 1379–1393.
Shaner NC, Campbell RE, Steinbach PA, Giepmans BNG, Palmer AE, Tsien RY (2004). Improved monomeric red, orange and yellow fluorescent proteins derived from Discosoma sp. red fluorescent protein. Nat Biotechnol 22, 1567–1572.
Shutova MS, Asokan SB, Talwar S, Assoian RK, Bear JE, Svitkina TM (2017). Self-sorting of nonmuscle myosins IIA and IIB polarizes the cytoskeleton and modulates cell motility. J Cell Biol 216, 2877–2889.
Shutova MS, Spessott WA, Giraudo CG, Svitkina TM (2014). Endogenous species of mammalian nonmuscle myosin IIA and IIB include activated monomers and heteropolymers. Curr Biol 24, 1958–1968.
Skau CT, Waterman CM (2015). Specification of architecture and function of actin structures by actin nucleation factors. Annu Rev Biophys 44, 285–310.
Small JV, Rottner K, Kaverina I, Anderson KI (1998). Assembling an actin cytoskeleton for cell attachment and movement. Biochim Biophys Acta 1404, 271–281.
Stam S, Alberts J, Gardel ML, Munro E (2015). Isoforms confer characteristic force generation and mechanosensation by myosin II filaments. Biophys J 108, 1997–2006.
Tang N, Ostap EM (2001). Motor domain-dependent localization of myo1b (myr-1). Curr Biol 11, 1131–1135.
Thomas DG, Yenepalli A, Denais CM, Rape A, Beach JR, Wang Y-L, Schiemann WP, Baskaran H, Lammerding J, Egelhoff TT (2015). Non-muscle myosin IIB is critical for nuclear translocation during 3D invasion. J Cell Biol 210, 583–594.
Titus MA (2017). Growing, splitting and stacking myosin II filaments. Nat Cell Biol 19, 77–79.
Tojkander S, Gateva G, Husain A, Krishnan R, Lappalainen P (2015). Generation of contractile actomyosin bundles depends on mechanosensitive actin filament assembly and disassembly. Elife 4, e06126.
Tojkander S, Gateva G, Lappalainen P (2012). Actin stress fibers-assembly, dynamics and biological roles. J Cell Sci 125, 1855–1864.
Tojkander S, Gateva G, Schevzov G, Hotulainen P, Naumanen P, Martin C, Gunning PW, Lappalainen P (2011). A molecular pathway for myosin II recruitment to stress fibers. Curr Biol 21, 539–550.
Totsukawa G, Yamakita Y, Yamashiro S, Hartshorne DJ, Sasaki Y, Matsumura F (2000). Distinct roles of ROCK (Rho-kinase) and MLCK in spatial regulation of MLC phosphorylation for assembly of stress fibers and focal adhesions in 3T3 fibroblasts. J Cell Biol 150, 797–806.
Uyeda TQP, Iwadate Y, Umeki N, Nagasaki A, Yumura S (2011). Stretching actin filaments within cells enhances their affinity for the myosin II motor domain. PLoS One 6, e26200.
Vallenius T (2013). Actin stress fibre subtypes in mesenchymal-migrating cells. Open Biol 3, 130001.
Vicente-Manzanares M, Koach MA, Whitmore L, Lamers ML, Horwitz AF (2008). Segregation and activation of myosin IIB creates a rear in migrating cells. J Cell Biol 183, 543–554.
Vicente-Manzanares M, Ma X, Adelstein RS, Horwitz AR (2009). Non-muscle myosin II takes centre stage in cell adhesion and migration. Nat Rev Mol Cell Biol 10, 778–790.
Vicente-Manzanares M, Newell-Litwa K, Bachir AI, Whitmore LA, Horwitz AR (2011). Myosin IIA/IIB restrict adhesive and protrusive signaling to generate front-back polarity in migrating cells. J Cell Biol 193, 381–396.
Vicente-Manzanares M, Zareno J, Whitmore L, Choi CK, Horwitz AF (2007). Regulation of protrusion, adhesion dynamics, and polarity by myosins IIA and IIB in migrating cells. J Cell Biol 176, 573–580.
Wang F, Kovács M, Hu A, Limouze J, Harvey EV, Sellers JR (2003). Kinetic mechanism of non-muscle myosin IIB: functional adaptations for tension generation and maintenance. J Biol Chem 278, 27439–27448.
Wei Q, Adelstein RS (2000). Conditional expression of a truncated fragment of nonmuscle myosin II-A alters cell shape but not cytokinesis in HeLa cells. Mol Biol Cell 11, 3617–3127.